THE JOURNAL OF BIOLOGICAL CHEMISTRY VOL. 286, NO. 11, pp. 9120–9126, March 18, 2011

Phosphomimetic Mutations Enhance Oligomerization of Phospholemman and Modulate Its Interaction with the Na/K-ATPase*

Received for publication, October 26, 2010, and in revised form, December 17, 2010 Published, JBC Papers in Press, January 10, 2011, DOI 10.1074/jbc.M110.198036

Qiujing Song[‡], Sandeep Pallikkuth[‡], Julie Bossuyt[§], Donald M. Bers[§], and Seth L. Robia[‡1]

From the [‡]Department of Cell and Molecular Physiology, Loyola University Chicago, Maywood, Illinois 60153 and the [§]Department of Pharmacology, University of California, Davis, California 95616

Na/K-ATPase (NKA) activity is dynamically regulated by an inhibitory interaction with a small transmembrane protein, phospholemman (PLM). Inhibition is relieved upon PLM phosphorylation. Phosphorylation may alter how PLM interacts with NKA and/or itself, but details of these interactions are unknown. To address this, we quantified FRET between PLM and its regulatory target NKA in live cells. Phosphorylation of PLM was mimicked by mutation S63E (PKC site), S68E (PKA/PKC site), or S63E/S68E. The dependence of FRET on protein expression in live cells yielded information about the structure and binding affinity of the PLM-NKA regulatory complex. PLM phosphomimetic mutations altered the quaternary structure of the regulatory complex and reduced the apparent affinity of the PLM-NKA interaction. The latter effect was likely due to increased oligomerization of PLM phosphomimetic mutants, as suggested by PLM-PLM FRET measurements. Distance constraints obtained by FRET suggest that phosphomimetic mutations slightly alter the oligomer quaternary conformation. Photon-counting histogram measurements revealed that the major PLM oligomeric species is a tetramer. We conclude that phosphorylation of PLM increases its oligomerization into tetramers, decreases its binding to NKA, and alters the structures of both the tetramer and NKA regulatory complex.

The sodium/potassium pump Na/K-ATPase (NKA)[2] is essential to establish the sodium/potassium concentration gradient across the plasma membrane (1). Besides being the foundation for the membrane potential, the sodium/potassium gradient created by NKA is the basis for many other cotransport and exchange processes (2). NKA plays a particularly important role in cardiac function. Disordered sodium/potassium handling is associated with heart disease (3), and targeting NKA with inhibitory drugs is one of the oldest, most effective treatments for the inadequate contractility of the failing heart (4). NKA is functionally regulated by PKA/PKC-dependent signaling pathways (1–6). These pathways impinge on phospholemman (PLM; or FXYD1), a 72-amino acid regulator of NKA in cardiac tissue (6–9). PLM inhibits NKA activity by reducing its apparent sodium affinity (8, 9). Tonic inhibition of NKA by PLM is relieved upon phosphorylation by PKA or PKC (10–13). Notably, deletion of PLM abolishes the PKA- or PKC-mediated regulation on NKA (10–13), emphasizing the central role of this regulatory interaction.

Recently, much progress has been made elucidating the structural basis for the functional regulation of NKA by PLM. NMR studies showed that PLM adopts an L-shaped structure with a single membrane span (14). The N-terminal half of the protein consists of an extracellular domain containing the signature Phe-*X*-Tyr-Asp (F*X*YD) motif, followed by a transmembrane α-helix. Another helical domain on the cytoplasmic side of the plasma membrane contains the phosphate-accepting residues Ser-63 (PKC site) and Ser-68 (PKA/PKC site) (9, 14). This positively charged domain appears to associate with the surface of the bilayer, but phosphorylation may trigger helix reorientation and thereby tune the interaction of PLM with NKA (14). Interestingly, PLM also interacts with itself to form oligomers; *in vitro* experiments suggest these are tetramers (15, 16). Although no major phosphorylation-dependent PLM structure changes were detected in NMR studies (17), we previously found that FRET from PLM to PLM was increased upon PLM phosphorylation (18, 19), whereas FRET from NKA to PLM was reduced (19). These previous FRET studies suggest that phosphorylation of PLM affects its binding interactions or the quaternary conformation of the bound complexes. The relative contributions of changed binding affinity and altered structure have not yet been dissected from one another.

In a previous study, we demonstrated that phosphomimetic mutations of phospholamban (PLB) increased its self-binding affinity and altered the structure of its regulatory complex with the sarco(endo)plasmic reticulum Ca^{2+}-ATPase (SERCA) (20). Although they are localized to different membrane structures and have different ion selectivity, the PLB/SERCA proteins are analogous to PLM/NKA. The secondary/tertiary structure and regulatory function of PLB are similar to those of PLM (although opposite in orientation). Likewise, SERCA closely resembles NKA. Possibly the mechanisms of PLM/NKA regulation parallel those of PLB/SERCA regulation. In this study, we quantify the effect of phosphorylation-mimicking mutations on

* This work was supported, in whole or in part, by National Institutes of Health Grants HL092321 and EB006061 (to S. L. R.). This work was also supported by American Heart Association Fellowship 0720098Z (to Q. S.) and the McCormick Foundation (to the Department of Cell and Molecular Physiology Multiphoton Imaging Facility).

[1] To whom correspondence should be addressed: Dept. of Cell and Molecular Physiology, 102/5689, Loyola University Chicago, 2160 S. 1st Ave., Maywood, IL 60153. Tel.: 708-216-2522; Fax: 708-216-6308; E-mail: srobia@lumc.edu.

[2] The abbreviations used are: NKA, Na/K-ATPase; PLM, phospholemman; PLB, phospholamban; SERCA, sarco(endo)plasmic reticulum Ca^{2+}-ATPase; CFP, cyan fluorescent protein; PCH, photon-counting histogram.

the structure and affinity of PLM regulatory complexes in live cells.

EXPERIMENTAL PROCEDURES

Constructs—PLM tagged with either cyan fluorescent protein (PLM-CFP) or YFP (PLM-YFP) at the intracellular C terminus and the CFP-NKAα1 construct (in which CFP is attached at the NKA intracellular N terminus) were described previously (18, 19). For these constructs, we have previously validated enzymatic function (pump currents), modulation by pump ligands and kinases, and interaction specificity (18, 19). These studies indicated the fluorescent protein fusion tag does not interfere with pump function. The fluorescent proteins used were monomeric variants containing the A206K mutation (21). The pseudo-phosphorylation mutants S63E (PKC site), S68E (PKA/PKC site), and S63E/S68E (both sites) were created using the QuikChange mutagenesis kit (Stratagene, La Jolla, CA). Phosphomimetic mutants were compared with the non-phosphorylatable controls S63A and S68A.

Cell Culture and Transfection—Stable 293 cell lines expressing CFP-NKAα1 fusion proteins were cultured in DMEM with 5% fetal bovine serum in 60-mm dishes for 24 h to achieve ~60% confluency. 15 μg of plasmid DNA encoding PLM-YFP was transfected into the stable CFP-NKAα1 cells using a mammalian cell transfection kit (Stratagene) as described previously (20, 22, 23). AAV-293 cells were transfected with PLM-YFP plasmid DNA (0.1 μg) or cotransfected with plasmid DNA encoding PLM-CFP (1 μg) and PLM-YFP (5 μg). 20–24 h after transfection, cells were detached via mild trypsinization and replated on poly-D-lysine-coated glass bottom culture dishes. After adhering to the surface for 1 h, the cells in DMEM were imaged for quantitative FRET or photon-counting histogram analysis.

Quantitative FRET—Cells were imaged with an inverted microscope (Nikon TE2000-U) equipped with a metal halide lamp, an APO 60×/1.49 numerical aperture objective, and a back-thinned CCD camera (iXon 887, Andor Technology, Belfast, Northern Ireland) as described previously (20, 22, 23). FRET between CFP- and YFP-labeled proteins was quantified by progressive acceptor-selective photobleaching of the entire microscopic field of observation as described previously (20, 22, 23). The progressive photobleaching protocol was as follows: 100-ms acquisition of CFP image and 40-ms acquisition of YFP image, followed by 10-s exposure to YFP-selective photobleaching (504/12 nm). The FRET efficiency (E) was calculated for each cell according to the percentile change of CFP intensity (F) after YFP-selective photobleaching, *i.e.* $E = 1 - (F_{\text{pre-bleach}}/F_{\text{post-bleach}})$, and the FRET efficiency was plotted cell-by-cell according to the pre-bleach YFP fluorescence, which was taken as an index of the relative protein concentration of each cell. The protein concentration dependence of FRET efficiency was fit to a hyperbolic curve of the form $Y = (\text{FRET}_{\text{max}})X/(K_D + X)$, where Y is the FRET efficiency observed, and X is the protein concentration in the cell in arbitrary units. The maximal FRET (FRET_{max}) represents the intrinsic FRET of the protein complex. K_D is the dissociation constant (in arbitrary units) of the complexes, which measures their apparent binding affinity. K_{D1} is the dissociation constant of the PLM-PLM oligomer, and K_{D2} is the apparent dissociation constant of the PLM-NKA regulatory complex. For each mutant, values of K_D and FRET_{max} were summarized as a weighted mean (Equation 1), where SE is the standard error of the hyperbolic fit with respect to that parameter.

$$\bar{\chi} = \frac{\sum_{i=1}^{n} (\chi_i / SE_i^2)}{\sum_{i=1}^{n} (1/SE_i^2)} \quad \text{(Eq. 1)}$$

The standard error of the weighted mean was calculated according to Equation 2.

$$SE_{\bar{x}} = \sqrt{\frac{1}{\sum_{i=1}^{n} (1/SE_i^2)}} \quad \text{(Eq. 2)}$$

The z-score for a standard normal distribution was calculated for statistical comparisons between mutants according to Equation 3, where $p < 0.05$ was considered significant.

$$z = \frac{\bar{x}_1 - \bar{x}_2}{\sqrt{(SE_{\bar{x}_1})^2 + (SE_{\bar{x}_2})^2}} \quad \text{(Eq. 3)}$$

For the regulatory complex, the donor-acceptor separation distance was calculated according to $R = R_0((1/\text{FRET}_{\text{max}}) - 1)^{1/6}$ (24). For the PLM oligomer, the average donor-acceptor separation distance was calculated from FRET_{max} using a computational model of intra-oligomeric FRET (25) as described previously (20, 23). This model assumes a ring-shaped arrangement of subunits, which we regard as the most likely geometry (26). For values of $R \geq R_0$, FRET efficiency is strongly dependent on donor-acceptor separation distance and only weakly dependent on the number of subunits in the complex (25). The ratio of donors and acceptors in the oligomer was determined from the relative intensities of pre-photobleaching YFP emission and post-photobleaching CFP emission as described previously (20).

Photon-counting Histogram Analysis—Photon counting of PLM-YFP in live AAV-293 cells was performed with a confocal microscope (TCS-SP5, Leica Microsystems) using 512 nm excitation with an argon ion continuous wave laser that was attenuated to prevent photobleaching. Fluorescence emission was collected with a 63× water immersion objective (HCX PL APO, 1.2 numerical aperture) and band-pass filter (535–585 nm). Detection was performed with an avalanche photodiode (SPCM-AQRH, PerkinElmer Life Sciences) and a photon-counting card (ISS Inc.). Photon-counting histograms (PCH) were generated by ISS Vista software using a time bin width of 100 μs, which was much shorter than the translational diffusion time of the molecule in the cell. Fluorescence traces were integrated for 100 s for each PCH curve. The excitation beam was parked at several different subcellular positions for each of many cells. The average fluorescence intensity at the point of measurement was taken as an indicator of the protein concentration at that position. PCH curves were fitted with a nonlinear curve fitting routine using a one- or two-species model (27). A one-photon three-dimensional Gaussian model was assumed

for the excitation volume in our experiments. Resolution of diffusible species was accomplished by global analysis of several measurements of similar average fluorescence intensity, yielding molecular brightness (ϵ) and the concentration of each species (28, 29). Cell autofluorescence was determined to be negligible for this analysis.

RESULTS

Plasma Membrane Localization of Fluorescent Protein-fused PLM and NKAα1—Fig. 1 (*A–C*) shows that the fluorescence of the PLM fusion construct S63A was predominantly localized to the plasma membrane, with a small amount detectable in internal membrane structures. All other PLM variants showed the same localization pattern (data not shown). CFP-NKAα1 fusion proteins stably expressed in HEK293 cells also showed predominantly plasma membrane localization (Fig. 1*D*), and in cells transfected with PLM S63A-YFP (Fig. 1*E*), the proteins were highly co-localized (Fig. 1*F*).

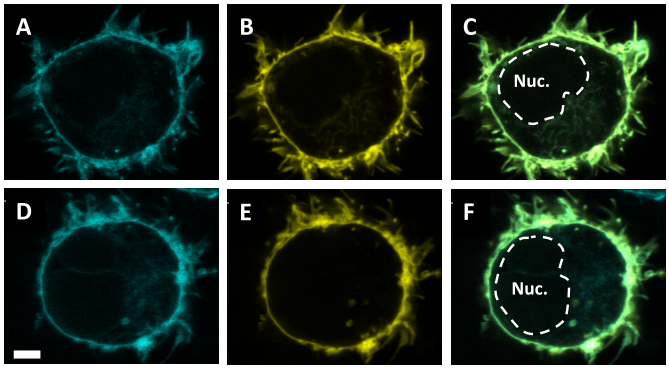

FIGURE 1. **Plasma membrane localization of fluorescent protein-fused PLM and NKA constructs in transfected cells.** *A–C*, images of cell expressing both PLM-CFP and PLM-YFP. *A*, PLM-CFP; *B*, PLM-YFP; *C*, merged PLM-CFP and PLM-YFP. *D–F*, images of cell expressing both CFP-NKAα1 and PLM-YFP. *D*, CFP-NKAα1; *E*, PLM-YFP; *F*, merged CFP-NKAα1 and PLM-YFP. *Nuc.*, nucleus. *Scale bar* = 5 μm. Optical sections of 0.9-μm thickness were obtained at a *z*-height corresponding to the center of the cell (~10 μm from the substrate).

PLM-NKA Regulatory Complex FRET—To investigate the effect of pseudo-phosphorylation mutations on the structure and apparent affinity of the PLM-NKA regulatory complex, we measured FRET between CFP-NKAα1 and PLM mutants labeled with YFP. Consistent with our previous study (18, 19), the mean FRET (average FRET observed for a large population of cells) was reduced for phosphomimetic mutants compared with non-phosphorylatable controls (Table 1). To dissect the relative contributions of changes in structure and binding affinity, we compared the FRET efficiency measured for each cell with the pre-bleach YFP fluorescence intensity (an index of protein concentration). Cell-to-cell variation in expression resulted in a wide range of protein concentrations. FRET increased with protein expression level, approaching a maximum (Fig. 2, *A* and *B*). Fitting with a hyperbola yielded $FRET_{max}$ and the concentration at which half-maximal FRET was observed (K_{D2}). The latter is the apparent dissociation constant and is inversely related to the affinity of PLM-NKA. The measured values of $FRET_{max}$ and K_{D2} are summarized in Fig. 2 (*C* and *D*) and Table 1. K_{D2} was increased by 75% by phosphomimetic mutations of the PKC site (S63E), the PKA/PKC site (S68E), or both sites (S63E/S68E) compared with the non-phosphorylatable mutants (S63A and S68A). This is evident in Fig. 2 (*A* and *B*) as a right-shifted dependence of FRET on protein expression relative to non-phosphorylatable controls. A comparison of measured K_{D2} values is provided in Fig. 2*D*. The results suggest that PLM binding to NKA is reduced by phosphomimetic mutations. Notably, $FRET_{max}$ was decreased by 20% by phosphomimetic mutations (Fig. 2*C*). The changes in $FRET_{max}$ are consistent with a conformational change in the regulatory complex.

PLM Oligomer FRET—To investigate the effect of pseudo-phosphorylation mutations on the structure and affinity of the PLM oligomer, we measured FRET between PLM-CFP and PLM-YFP. Intra-oligomer FRET efficiency increased with protein concentration as shown in Fig. 3 (*A* and *B*). $FRET_{max}$ of

TABLE 1

Summary of effects of phosphomimetic mutations of PLM

Data are means ± S.E. Distance constraints were calculated from the Forster equation (for PLM-NKA) or a computational model of FRET within a ring-shaped oligomer (for PLM-PLM FRET). The parameter ϵ is the molecular brightness obtained from a fit of the PCH. a.u., arbitrary units.

	S63A	S63E	S68A	S68E	S63E/S68E
PLM-NKA complex					
Mean FRET (%)	14.5 ± 1.3	9.3 ± 0.8[a]	15.3 ± 1.1	10.5 ± 1.2[b]	9.4 ± 1.1[b]
$FRET_{max}$ (%)	19.9 ± 0.6	16.0 ± 0.7[a]	19.9 ± 1.0	16.1 ± 1.0[b]	15.8 ± 0.9[b]
Acceptor mole fraction	0.93 ± 0.04	0.90 ± 0.04	0.91 ± 0.02	0.91 ± 0.03	0.93 ± 0.05
CFP-YFP separation distance (Å)	64.6 ± 0.5	68.2 ± 0.8[a]	64.6 ± 0.8	68.1 ± 1.1[b]	68.4 ± 1.0[b]
Apparent K_{D2} (a.u.)	6.8 ± 0.7	12.2 ± 1.0[a]	7.6 ± 1.0	13.2 ± 1.5[b]	12.4 ± 1.7[b]
n (set of experiments)	3	3	4	3	3
N (number of cells)	390	313	296	273	439
PLM oligomer					
Mean FRET (%)	38.3 ± 1.7	32.4 ± 0.7[a]	37.7 ± 0.5	34.2 ± 0.4[b]	29.8 ± 0.8[b]
$FRET_{max}$ (%)	50.2 ± 2.1	46.2 ± 1.1[a]	50.6 ± 1.6	44.6 ± 1.3[b]	46.4 ± 1.4[b]
Acceptor mole fraction	0.89 ± 0.05	0.92 ± 0.03	0.93 ± 0.01	0.91 ± 0.01	0.94 ± 0.01
CFP-YFP separation distance (Å)	57.5 ± 0.4	59.2 ± 0.2[a]	57.9 ± 0.3	59.7 ± 0.2[b]	59.4 ± 0.3[b]
K_{D1} (a.u.)	10.4 ± 1.5	5.4 ± 0.6[a]	11.6 ± 0.9	6.4 ± 0.6[b]	6.5 ± 0.5[b]
n (set of experiments)	3	3	8	6	7
N (number of cells)	354	274	479	423	223
PLM oligomer PCH					
ϵ_1 (species 1; counts/bin)	0.22 ± 0.01	0.23 ± 0.01	0.23 ± 0.01	0.23 ± 0.01	0.23 ± 0.01
ϵ_2 (species 2; counts/bin)	0.88 ± 0.04	0.87 ± 0.04	0.85 ± 0.04	0.85 ± 0.04	0.85 ± 0.04
Brightness ratio (ϵ_2/ϵ_1)	4	3.8	3.7	3.7	3.7

[a] $p < 0.05$ *versus* S63A.
[b] $p < 0.05$ *versus* S68A.

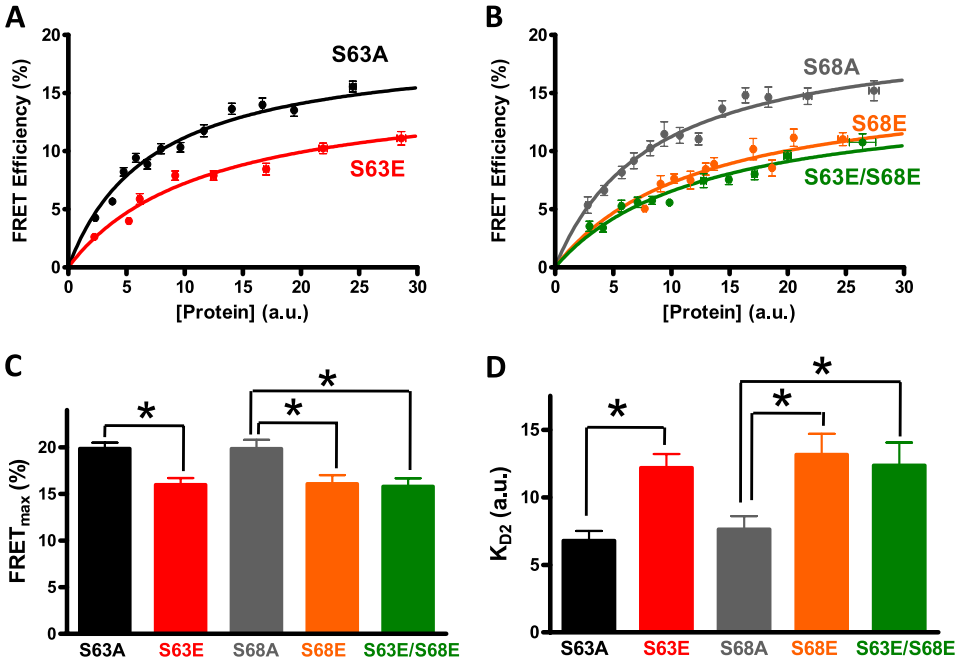

FIGURE 2. **Effects of phosphomimetic mutations on PLM-NKA FRET.** *A*, concentration dependence of FRET for S63A (*black circles*) and S63E (*red circles*). *a.u.*, arbitrary units. *B*, concentration dependence of FRET for S68A (*gray circles*), S68E (*orange circles*), and S63E/S68E (*green circles*). The concentration dependence of FRET was well described by a hyperbola of the form FRET = FRET$_{max}$[protein]/(K_{D2} + [protein]). *C* and *D*, mean FRET$_{max}$ and K_{D2} parameters, respectively, obtained by hyperbolic fitting of data from multiple independent experiments. Values are means ± S.E. *, $p < 0.05$ *versus* S63A or S68A.

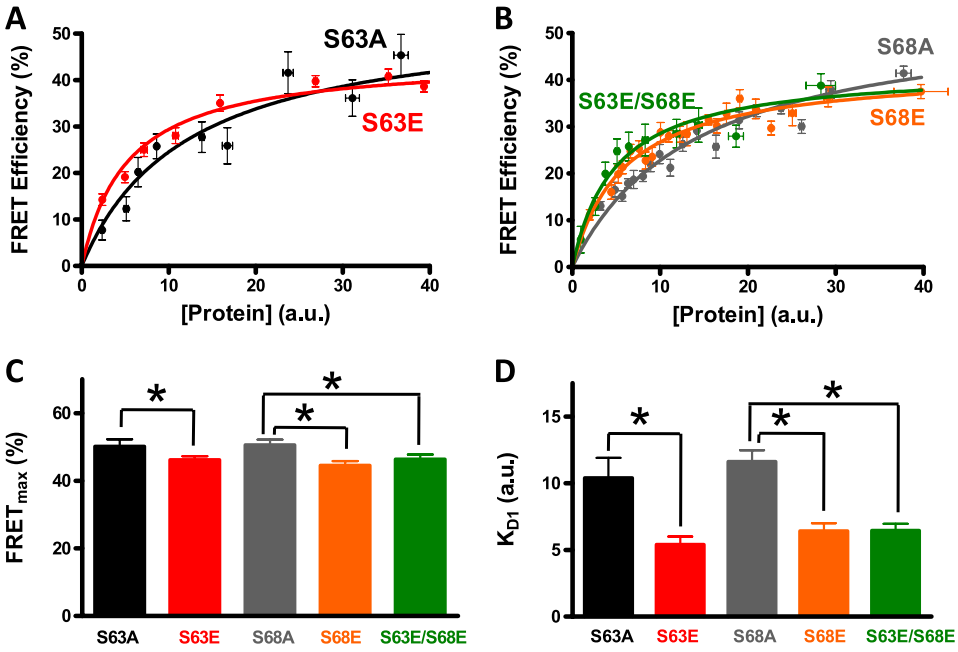

FIGURE 3. **Effects of phosphomimetic mutations on PLM-PLM FRET.** *A*, concentration dependence of FRET for S63A (*black circles*) and S63E (*red circles*). *a.u.*, arbitrary units. *B*, concentration dependence of FRET for S68A (*gray circles*), S68E (*orange circles*), and S63E/S68E (*green circles*). The concentration dependence of FRET was well described by a hyperbola of the form FRET = FRET$_{max}$[protein]/(K_{D1} + [protein]). *C* and *D*, mean FRET$_{max}$ and K_{D1} parameters, respectively, obtained by hyperbolic fitting of data from multiple independent experiments. Values are means ± S.E. *, $p < 0.05$ *versus* S63A or S68A.

PLM phosphomimetic mutants was modestly reduced by 9% (Fig. 3*C*). The PLM oligomer dissociation constant (K_{D1}) was reduced by 45% by phosphomimetic mutations as shown in Fig. 3*D* and Table 1. The data suggest increased PLM oligomerization after pseudo-phosphorylation, combined with a small change in the conformation of the oligomeric complex.

PCH Analysis—To investigate PLM oligomerization at very low concentrations, we generated PCHs of PLM-YFP expressed in live cells. Fig. 4*A* shows representative histograms of PLM mutants labeled with YFP. Although these data were obtained from subcellular regions with similar average fluorescence intensities, phosphomimetic mutants showed right-shifted histograms (Fig. 4*A*, *upper panel*). Histograms generated from dim cells (expressing a low concentration of protein) were well described by a single-species model with a molecular brightness of 0.23 counts/bin for all PLM mutants tested (Table 1). Bright

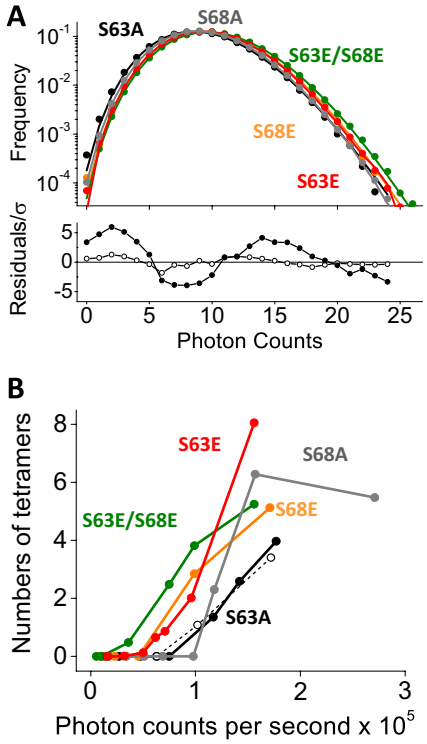

FIGURE 4. **Effects of phosphomimetic mutations on PLM molecular brightness.** *A*, *upper panel*, PCH curves recorded from regions with similar fluorescence intensities in cells expressing mutants of PLM labeled with YFP. The *abscissa* is the *Photon Counts*, or the numbers of photons detected in a time bin of 100 μs. The *ordinate* is the *Frequency*, or the fraction of bins with a particular photon count. The data were well described by a fit for two species with a 4-fold difference in brightness. *Lower panel*, the fit residuals, divided by standard deviation (σ), for a one-species fit (*closed circles*) and a two-species fit (*open circles*) (representative S68A data). *B*, average number of tetramers detected in the observation volume for a 100-μs bin time *versus* the average fluorescence intensity of that sample expressed as photon flux (counts/s). S63A tetramer concentration plots obtained by sampling different cells (*black closed circles*) were similar to those obtained by sampling different regions of the same cell (*black open circles*). Values are means ± S.E.

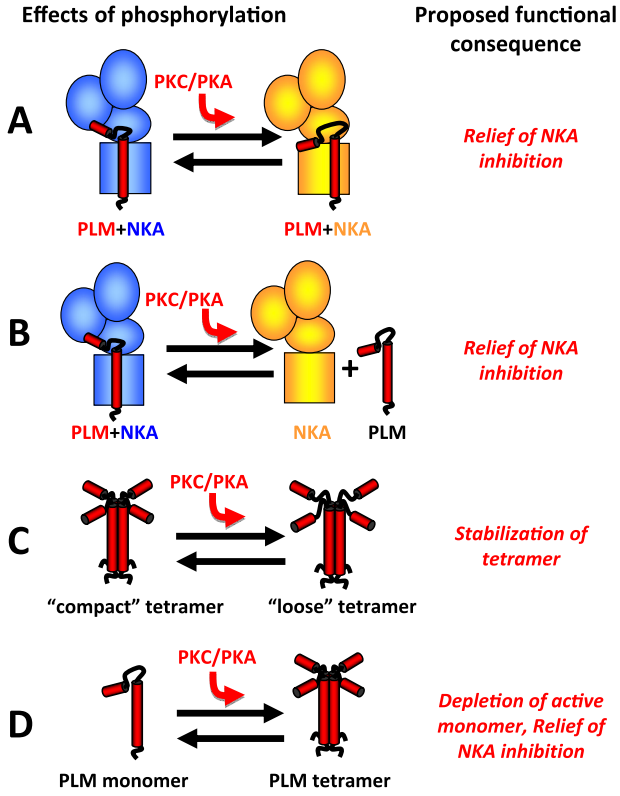

FIGURE 5. **Scheme for regulation of NKA by PLM.** Shown are the effects of phosphorylation of PLM and the likely functional consequences. *A*, regulatory complex structure transition away from a compact (inhibited) structure; *B*, decreased PLM-NKA binding; *C*, PLM tetramer transition away from a compact structure; *D*, increased PLM tetramerization. This study suggests that unbinding of PLM from NKA (*B*) is an indirect result of increased PLM oligomerization (*D*).

cells (expressing a higher concentration of protein) gave PCH curves that were best described by a two-species model. A comparison of residuals from one- and two-species fits is provided in Fig. 4*A* (*lower panel*). The second species was characterized by a 4-fold higher molecular brightness (0.86 counts/bin), consistent with a tetramer (Table 1). Fig. 4*B* shows the number of bright species that were detected *versus* the average fluorescence intensity (photon counts/s) in the detection volume. The number of tetramers increased with fluorescence intensity, suggesting that tetramerization increases with protein concentration. A similar trend was observed whether measurements were taken from different cells (Fig. 4*B*, *black closed circles*) or from regions of differential brightness within the same cell (*black open circles*). The apparent effect of phosphomimetic mutations was to reduce the critical concentration at which the tetrameric species began to be observed.

DISCUSSION

The present observations relating to PLM structure and affinity provide insight into the mechanism of kinase regulation of NKA inhibition by PLM. We propose that relief of pump inhibition is due to a combination of conformational changes (Fig. 5, *A* and *C*) and dynamic shifts in regulatory binding equilibria (Fig. 5, *B* and *D*). The effects of phosphorylation include the following: a conformational change in the PLM-NKA regulatory complex (Fig. 5*A*), decreased binding of PLM to NKA (Fig. 5*B*), a conformational change in the PLM tetramer (Fig. 5*C*), and increased oligomerization of PLM (Fig. 5*D*).

PLM-NKAα1 Structure and Equilibrium—The concentration dependence of PLM-NKAα1 FRET provides $FRET_{max}$ of the regulatory complex, which is taken to represent the intrinsic FRET efficiency of the complex. As far as can be detected by FRET, CFP-NKAα1 and PLM-YFP compose a bimolecular complex (18). Therefore, the donor-acceptor separation distance can be obtained from $FRET_{max}$ by the relationship $R = R_0((1/FRET_{max}) - 1)^{1/6}$ (24). Assuming random relative dipolar orientations ($\kappa^2 = 2/3$) and accounting for 4% nonspecific energy transfer, the measured intrinsic FRET efficiencies correspond to CFP-YFP separation distances of 64.6 Å for the non-phosphorylatable mutants. The phosphomimetic mutants S63E, S68E, and S63E/S68E had an average donor-acceptor separation distance of 68.3 Å. We conclude that phosphomimetic mutations alter the structure of the bound PLM-NKA complex. This putative structure change is similar in magnitude to other conformational changes measured by FRET (30–32). The structure transition is represented schematically in Fig. 5*A* as a change from an inactive (*blue*) to an active (*orange*) PLM-NKA complex. The uncertain disposition of the fluorescent protein tags limits quantitative interpretation of FRET

constraints. However, the large probe separation distances determined here (~65 Å) are compatible with crystal structures (33) and computational models (14) in which the PLM-binding site and the NKA N terminus (CFP fusion site) are on opposite sides of NKA. A similar arrangement has been proposed for the analogous regulatory complex of SERCA with its conjugate regulatory partner PLB (34). We have previously determined probe separation distances of 58–65 Å for the PLB-SERCA complex (20, 22, 23). Moreover, the magnitude and direction of the distance change after phosphomimetic mutations were the same (+4 Å) for both regulatory complexes (20). The data underscore the structural similarity of the respective regulatory complexes and suggest that similar regulatory mechanisms may govern both pumps.

All PLM phosphomimetic mutants showed saturable binding to NKAα1 (Fig. 2, *A* and *B*), suggesting that relief of NKA inhibition with phosphorylation does not require complete dissociation of the regulatory complex. However, the right-shifted concentration dependence for phosphomimetic mutants (*versus* S68A or S63A) indicates a reduced apparent affinity for NKA (higher K_{D2}). It is noteworthy that single phosphomimetic mutants showed the same magnitude of K_{D2} shift and structure change as the double mutant S63E/S68E, suggesting that the Ser-63 and Ser-68 phosphorylation sites are redundant. Both the structure change (decreased $FRET_{max}$) (Fig. 2*C*) and apparent affinity change (increased K_{D2}) (Fig. 2*D*) may contribute to the regulation of NKA by PLM phosphorylation. The relative functional prominence of the two mechanisms *in vivo* is unknown.

It is important to note that the YFP fluorescence intensity measurements used as an index of protein concentration (Fig. 2, *A* and *B*) include both the monomeric and oligomeric forms of PLM-YFP. Thus, the PLM-NKAα1 equilibrium may be influenced by changes in the PLM oligomerization equilibrium. To determine whether the observed increase in K_{D2} was a direct change in the intrinsic affinity of monomeric PLM for NKA (Fig. 5*B*) or an indirect result of decreased K_{D1} (Fig. 5*D*), we also measured FRET between fluorescent probes on different subunits of the PLM oligomer.

PLM Oligomer Structure and Equilibrium—Using a computational model (20) of FRET within a ring-shaped oligomer (25), we calculated an average probe separation distance of 58 Å for the non-phosphorylatable PLM mutants. This is a rather large distance, as may be expected from the L-shaped structure of PLM that was determined by NMR (35). The PLM oligomer may assume a structure analogous to the PLB pentamer (36, 37), in which the cytoplasmic domains point outward from a central hub of transmembrane helices. However, the relative positions of the PLM cytoplasmic domain and the fluorescent protein chromophore are not known precisely, so we cannot rule out alternative conformations. The observed decrease in PLM oligomer $FRET_{max}$ after phosphomimetic mutations (Fig. 3*C*) is consistent with a modest increase in average probe separation distance from 58 to 60 Å. This represents a very small change in the oligomeric architecture. The results underscore the value of long-range distance constraints for measuring subtle conformational changes in macromolecules. For simplicity, the change in the structure with phosphorylation is represented schematically in Fig. 5*C* as shifting away from a "compact" conformation, but other structural effects could be envisioned. For example, phosphorylation may cause increased membrane association or a change in the dynamics of the PLM cytoplasmic domain (14). The functional significance of the apparent conformational change is unclear because the role of the oligomer is not proven. One possibility is that the oligomeric species is a reserve pool, which does not bind or regulate NKA (19). The role of the putative structure change may be to stabilize the assembled complex, increasing the oligomer population at the expense of the inhibitory monomeric species. We found that all three phosphomimetic mutations favor PLM oligomerization in the membranes of live cells, increasing binding affinity by ~2-fold (Fig. 3*D*). As we observed for the regulatory complex (Fig. 2*D*), there was no additional effect for the double mutant compared with single mutations. The data suggest that phosphorylation of either site is sufficient for full regulation of PLM oligomerization. It is noteworthy that the changes in K_{D1} (Fig. 3*D*) and K_{D2} (Fig. 2*D*) are of similar magnitude and opposite direction (1.8-fold difference) (Table 1). The data suggest that unbinding of PLM from NKA (Fig. 5*B*) is not a consequence of a change in the intrinsic affinity of PLM monomers for the pump (K_{D2}) but rather is an indirect effect of increased PLM oligomerization (Fig. 5*D*). A similar concerted change in linked equilibria was observed for PLB-binding interactions (20, 38). In response to analogous phosphomimetic mutations, PLB K_{D1} and K_{D2} showed 2.1- and 1.9-fold changes, respectively (20). PLB oligomerization interactions are apparently more avid than those of PLM. This may be why PLB oligomers are visible by SDS-PAGE, whereas PLM runs as a monomer.

PCH Analysis—Conclusions derived from FRET experiments were supported by the results of complementary PCH experiments (Fig. 4). A PCH is generated by counting photons emitted from diffusible fluorescent species as they pass through the excitation/detection volume of a parked laser beam of a confocal microscope. This method allows determination of the molecular brightness (ϵ) and the absolute concentration of the fluorescent species in the observation volume (28). It is useful for probing the oligomerization states of proteins in living cells (27, 29) with submicron spatial resolution. In these experiments, two diffusible species were observed, with an ~4-fold difference in molecular brightness (Table 1). The data are compatible with a mixture of monomers and tetramers. That the major oligomeric species is a tetramer was previously suggested by *in vitro* experiments of another group (15, 16, 26) and is consistent with our own observation (in FRET experiments) that the oligomer size is three or more protomers (18). We found that the concentration of tetramers increased with average fluorescence intensity (Fig. 4*B*). These data are analogous to the FRET efficiency *versus* concentration binding curves given in Fig. 3 (*A* and *B*), although the PCH technique is applicable to a much lower concentration range. The effect of phosphomimetic mutations was to reduce the threshold concentration at which the tetrameric species were observed. Notably, differential oligomerization was observed in different subcellular regions of the same cell (Fig. 4*B*, *black open circles*). The results mimicked the pattern of concentration-dependent oligomerization observed by sampling separate cells with different fluo-

rescence intensity (Fig. 4*B*, *black closed circles*). Subcellular regions with the highest fluorescence intensity had the highest numbers of tetramers and the highest tetramer/monomer ratio. Dim regions were dominated by the monomeric species. The final balance of tetramers and monomers *in vivo* must be determined by the steady-state concentration at the plasma membrane. In this regard, tetramers began to be detected at a fluorescence intensity of 1×10^5 photon counts/s, which corresponds to an average concentration of ~25 YFP molecules in the excitation volume. Assuming that the plane of the bilayer bisects the excitation volume, this suggests a membrane density of 30 PLM-YFP molecules/μm^2. Although the concentration of PLM *in vivo* is unknown, it is probably similar to the density of NKA in cardiac myocyte sarcolemma, which has been variously estimated as 320 (39), 1200 (40), and 2600 (41) pumps/μm^2. We conclude that oligomerization of PLM occurs at expression levels that are well below the expected *in vivo* concentration. Taken together with the observation that PLM-PLM binding affinity is comparable with the affinity of the PLM-NKA interaction (Table 1), the results suggest that PLM oligomerization does occur *in vivo*.

Summary—The conclusions of this study are summarized in Fig. 5. We propose that the major PLM oligomeric species is a tetramer. After phosphorylation of either Ser-63 or Ser-68, the PLM tetramer undergoes a structure transition (Fig. 5*C*), slightly increasing the separation of the cytoplasmic domains and enhancing tetramer stability. This increases PLM oligomerization (Fig. 5*D*), which is observed as a reduction in K_{D1}. As a consequence of increased PLM oligomerization, the pool of monomeric PLM is depleted, which indirectly affects apparent K_{D2}. The result is reduced binding of PLM to NKA (Fig. 5*B*) and therefore reduced inhibition of NKA by PLM. Phosphorylation of PLM also alters the conformation of the PLM-NKA regulatory complex (Fig. 5*A*), increasing the separation of the PLM cytoplasmic domain and the NKA N terminus by 4 Å. Of these effects, we regard the structural rearrangement of the regulatory complex (Fig. 5*A*) and the unbinding of PLM from NKA (Fig. 5*B*) as most directly relevant to NKA regulation.

Acknowledgments—We thank Zhanjia Hou and Kiranpreet Kaur for technical assistance and Ramon Durazo-Arvizu for assistance with statistical analyses.

REFERENCES

1. Cornelius, F., and Mahmmoud, Y. A. (2003) *Ann. N.Y. Acad. Sci.* **986,** 579–586
2. Faller, L. D. (2008) *Arch. Biochem. Biophys.* **476,** 12–21
3. Verdonck, F., Volders, P. G., Vos, M. A., and Sipido, K. R. (2003) *J. Mol. Cell. Cardiol.* **35,** 5–25
4. Lingrel, J. B. (2010) *Annu. Rev. Physiol.* **72,** 395–412
5. Fuller, W., Howie, J., McLatchie, L. M., Weber, R. J., Hastie, C. J., Burness, K., Pavlovic, D., and Shattock, M. J. (2009) *Am. J. Physiol. Cell Physiol.* **296,** C1346–C1355
6. Therien, A. G., and Blostein, R. (2000) *Am. J. Physiol. Cell Physiol.* **279,** C541–C566
7. Bers, D. M., and Despa, S. (2009) *Trends Cardiovasc. Med.* **19,** 111–118
8. Crambert, G., Fuzesi, M., Garty, H., Karlish, S., and Geering, K. (2002) *Proc. Natl. Acad. Sci. U.S.A.* **99,** 11476–11481
9. Shattock, M. J. (2009) *Curr. Opin. Pharmacol.* **9,** 160–166
10. Bell, J. R., Kennington, E., Fuller, W., Dighe, K., Donoghue, P., Clark, J. E., Jia, L. G., Tucker, A. L., Moorman, J. R., Marber, M. S., Eaton, P., Dunn, M. J., and Shattock, M. J. (2008) *Am. J. Physiol. Heart Circ. Physiol.* **294,** H613–H621
11. Despa, S., Bossuyt, J., Han, F., Ginsburg, K. S., Jia, L. G., Kutchai, H., Tucker, A. L., and Bers, D. M. (2005) *Circ. Res.* **97,** 252–259
12. Despa, S., Tucker, A. L., and Bers, D. M. (2008) *Circulation* **117,** 1849–1855
13. Han, F., Bossuyt, J., Despa, S., Tucker, A. L., and Bers, D. M. (2006) *Circ. Res.* **99,** 1376–1383
14. Franzin, C. M., Gong, X. M., Teriete, P., and Marassi, F. M. (2007) *J. Bioenerg. Biomembr.* **39,** 379–383
15. Beevers, A. J., and Kukol, A. (2006) *Protein Sci.* **15,** 1127–1132
16. Wong, A., Beevers, A. J., Kukol, A., Dupree, R., and Smith, M. E. (2008) *Solid State Nucl. Magn. Reson.* **33,** 72–75
17. Teriete, P., Thai, K., Choi, J., and Marassi, F. M. (2009) *Biochim. Biophys. Acta* **1788,** 2462–2470
18. Bossuyt, J., Despa, S., Han, F., Hou, Z., Robia, S. L., Lingrel, J. B., and Bers, D. M. (2009) *J. Biol. Chem.* **284,** 26749–26757
19. Bossuyt, J., Despa, S., Martin, J. L., and Bers, D. M. (2006) *J. Biol. Chem.* **281,** 32765–32773
20. Hou, Z., Kelly, E. M., and Robia, S. L. (2008) *J. Biol. Chem.* **283,** 28996–29003
21. Zacharias, D. A., Violin, J. D., Newton, A. C., and Tsien, R. Y. (2002) *Science* **296,** 913–916
22. Hou, Z., and Robia, S. L. (2010) *J. Mol. Biol.* **402,** 210–216
23. Kelly, E. M., Hou, Z., Bossuyt, J., Bers, D. M., and Robia, S. L. (2008) *J. Biol. Chem.* **283,** 12202–12211
24. Forster, T. (1948) *Ann. Phys.* **2,** 55–75
25. Li, M., Reddy, L. G., Bennett, R., Silva, N. D., Jr., Jones, L. R., and Thomas, D. D. (1999) *Biophys. J.* **76,** 2587–2599
26. Beevers, A. J., and Kukol, A. (2007) *J. Biol. Chem.* **282,** 32742–32748
27. Chen, Y., Wei, L. N., and Müller, J. D. (2003) *Proc. Natl. Acad. Sci. U.S.A.* **100,** 15492–15497
28. Chen, Y., Müller, J. D., So, P. T., and Gratton, E. (1999) *Biophys. J.* **77,** 553–567
29. Müller, J. D., Chen, Y., and Gratton, E. (2000) *Biophys. J.* **78,** 474–486
30. Karasawa, A., Tsuboi, Y., Inoue, H., Kinoshita, R., Nakamura, N., and Kanazawa, H. (2005) *J. Biol. Chem.* **280,** 41900–41911
31. Marcaggi, P., Mutoh, H., Dimitrov, D., Beato, M., and Knöpfel, T. (2009) *Proc. Natl. Acad. Sci. U.S.A.* **106,** 11388–11393
32. Papadopoulos, S., Leuranguer, V., Bannister, R. A., and Beam, K. G. (2004) *J. Biol. Chem.* **279,** 44046–44056
33. Shinoda, T., Ogawa, H., Cornelius, F., and Toyoshima, C. (2009) *Nature* **459,** 446–450
34. Toyoshima, C., Asahi, M., Sugita, Y., Khanna, R., Tsuda, T., and MacLennan, D. H. (2003) *Proc. Natl. Acad. Sci. U.S.A.* **100,** 467–472
35. Teriete, P., Franzin, C. M., Choi, J., and Marassi, F. M. (2007) *Biochemistry* **46,** 6774–6783
36. Robia, S. L., Flohr, N. C., and Thomas, D. D. (2005) *Biochemistry* **44,** 4302–4311
37. Traaseth, N. J., Verardi, R., Torgersen, K. D., Karim, C. B., Thomas, D. D., and Veglia, G. (2007) *Proc. Natl. Acad. Sci. U.S.A.* **104,** 14676–14681
38. Cornea, R. L., Jones, L. R., Autry, J. M., and Thomas, D. D. (1997) *Biochemistry* **36,** 2960–2967
39. Colvin, R. A., Ashavaid, T. F., and Herbette, L. G. (1985) *Biochim. Biophys. Acta* **812,** 601–608
40. Bers, D. M. (2002) *Excitation-Contraction Coupling and Cardiac Contractile Force*, 2nd Ed., p. 90, Kluwer Academic Publishers, Dordrecht, The Netherlands
41. Dobretsov, M., Hastings, S. L., and Stimers, J. R. (1998) *J. Physiol.* **507,** 527–539